The effect of reactor pressure on the electrical and structural properties of InN epilayers grown by high-pressure chemical vapor deposition

M. K. I. Senevirathna[a)], S. Gamage, R. Atalay, A. R. Acharya, A. G. U. Perera and N. Dietz
Department of Physics and Astronomy, Georgia State University, Atlanta, GA 30303

M. Buegler, A. Hoffmann
Institut für Festkörperphysik, Technische Universität Berlin, Berlin, Germany

L. Su, A. Melton, I. Ferguson
Dept. Electrical & Computer Engineering, University of North Carolina Charlotte, NC 28223

The influence of super-atmospheric reactor pressures (2.5-18.5 bar) on the electrical and structural properties of InN epilayers deposited on GaN/sapphire (0001) templates by high-pressure Chemical Vapor Deposition has been studied. The epilayers were analyzed by Raman, x-ray diffraction (XRD), and Fourier transform infrared reflectance spectrometry to determine the structural properties as well as the phonon frequencies, dielectric function, plasma frequency, layer thickness and damping parameters of the epilayers. For the studied process parameter space, best material properties were achieved at a reactor pressure of 12.5 bar and a group V/III ratio of 2500 with a free carrier concentration of 1.5×10^{18} cm^{-3}, a mobility of the bulk InN layer of 270 $cm^2V^{-1}s^{-1}$, and a Raman (E_2 high) FWHM value of 10.3 cm^{-1}. This study shows that the crystalline layer properties probed by XRD $2\theta-\omega$ scans improve with increasing reactor pressure.

I. INTRODUCTION

Indium nitride (InN) and indium-rich group III-nitride alloys are of renowned interest due to their potential in high-speed (THz-regime) device structures, for high-efficient energy conversion devices such as photovoltaic cells and various light emitting device structures.[1] Therefore, understanding and optimizing of the material properties as a function of growth process conditions are of crucial importance for fabrication of InN and indium-rich group III-nitride epilayers and heterostructures.[2]

As of today, the structural and optoelectronic properties of the binary InN vary widely depending on the growth process used. Under low-pressure metal-organic chemical vapor deposition (MOCVD, also denotes as OMCVD, OMVPE or MOVPE) conditions, the integration of InN epilayers with other group III-nitrides is challenged due to the low dissociation temperature of InN[1] (~600 °C) relative to that of GaN[3] (~1000 °C), which leads to stoichiometric instabilities[4, 5] and a potential immiscibility for ternary InGaN alloys.[6] In 1970, McChesney *et*

[a)]Electronic mail: mkindikas@phy-astr.gsu.edu

al.[5] assessed the use of high pressure as a potential pathway to stabilize the group III-nitrides and their alloys at higher growth temperatures under thermodynamic equilibrium conditions. Though thin film growth processes can employ various degrees of non-equilibria to stabilize epilayers, the regime of super-atmospheric CVD is still mostly unexplored for the growth of III-nitride alloys. At low-pressure MOCVD, the growth of InN is limited to growth temperatures at or below 600 °C,[7] requiring a high group-V/III precursor ratio due to the insufficient cracking of ammonia. In order to stabilize InN epilayers at higher growth temperatures that may allow for improved materials quality as well as the stabilization of indium-rich ternary InGaN heterostructures, we explore in this study the growth of InN by high-pressure chemical vapor deposition (HPCVD) at reactor pressures ranging from 2.5 bar and up to 20 bar. The details of the HPCVD rector system have been described previously.[8-11] For reactor pressures around 15 bar, the growth temperatures for InN are in the vicinity of 850 °C,[12] with group V/III precursor ratio from 1000 to 5000 explored. The smaller V/III precursor ratio compared to low-pressure MOCVD is due to the improved NH_3 decomposition kinetics at higher temperatures and gas densities. So far there are no studies that correlate the reactor pressure with the structural and electrical properties of InN epilayers grown by HPCVD which is the goal of this contribution. We present results on the influence of the rector pressure on the structural and optoelectronic properties of epitaxial InN layers, noting however that the reactor pressure is only one of the many process parameters that affects the properties of the epilayers.

II. EXPERIMENTAL

The InN epilayers were grown on GaN/Sapphire (0001) templates using a custom-built HPCVD reactor system. Ammonia (NH_3) and trimethylindium (TMI) were used as group-V and group-III precursors. The group-V/III molar precursor ratio was kept at ~ 2500, where the reactor pressure was varied between 2.5 and 18.5 bar. The total flow (carrier gas and reactants) was adjusted to maintain a constant flow velocity in the reaction zone, above the growth surface. The growth temperatures were adjusted for each reactor pressure to obtain optimum crystallinity. The growth temperature increases linearly with reactor pressure from 750 to 865 °C.[12] The InN deposition process consists of the following steps: First, the substrate was heated to the growth temperature and exposed to a constant ammonia flow of 1200 sccm for 5 min. Afterward, an InN nucleation layer was deposited with a group-V/III ratio of 2400 for 1 minute. This nucleation layer was annealed with a group-V/III flow ratio of 12000 for 1 min, which was immediately followed by the steady-state growth of the bulk InN epilayer grown with a group-V/III ratio of 2400. All these steps were done at the same temperature. The growth time for each samples was 90 min.

The grown InN epilayers were characterized by FTIR reflection measurements, Raman, and XRD measurements. The IR reflection measurements on the samples were performed in near normal incidence (~8°) configuration at room temperature using a Perkin-Elmer FTIR spectrophotometer, in the spectral range of 450-7000 cm^{-1} with the MCT (HgCdTe) detector and KBr beam splitter. The structural properties of the InN epilayers have been analyzed by X'pert Pro MRD PANalytical high-resolution x-ray diffraction spectrometer performing both on-axis as well as off-axis and by a custom built[13] Raman spectrometer utilizing a McPherson McTripleLE spectrometer system equipped with a 40X microscope lens. The Raman spectra were taken at

room temperature in unpolarized back-scattering geometry along the (0001) crystalline plane with excitation energy of 2.33 eV.

III. RESULTS AND DISCUSSION

The FWHM values of the InN (0002) XRD (2θ-ω scan) Bragg reflex as a function of the reactor pressure are depicted in the FIG. 1. With increasing reactor pressure the FWHM values decrease but show a wide statistical variance. In order to extensively study the crystalline quality of the samples, the off-axis measurements were also performed using XRD 2θ-ω scans. The correlation between the FWHM values of off-axis InN (2-102) with the reactor pressure is depicted in FIG. 2. A similar trend as for the on-axis scan is observed indicating an improved in plane structural quality. The Raman analysis of FWHM values for the Raman E_2(high) mode of the InN epilayers grown on GaN templates are exhibited in FIG. 3 as a function of reactor pressure.

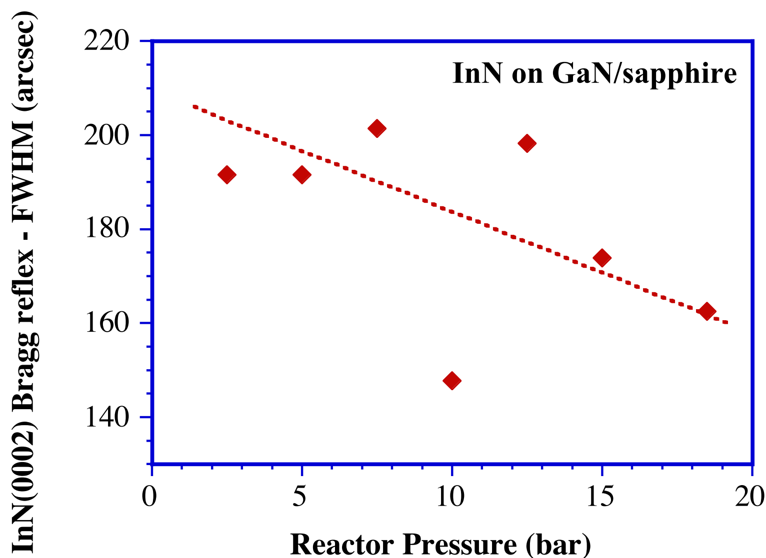

Figure 1. XRD FWHM (2θ -ω ω scan in triple crystal geometry) of InN peak ((0002) Bragg reflex at about 31.33°) as function of the reactor pressure.

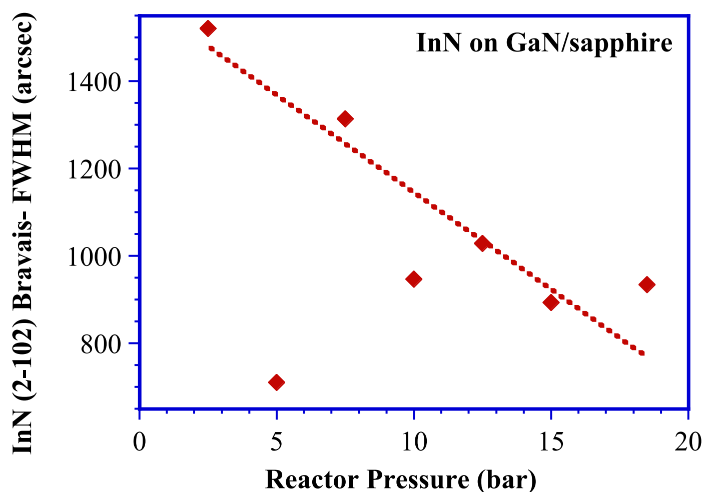

Figure 2. XRD FWHM (2θ-ω scan in triple crystal geometry) values of off-axis InN (2-102) of the InN epilayers as a function of reactor pressure.

The Raman E_2(high) mode position and FWHM values are microscopic measurements for the local strain and for the local crystalline structure and ordering perfection respectively, while

the position and the FWHM values of the InN (0002) XRD (2θ-ω scan) reflects the long range ordering and crystalline perfection in the InN epilayers. As shown in the FIG. 1, a sudden improvement of the FWHM value of the InN (0002) XRD (2θ-ω scan) is observed for the sample grown at 10 bar, a phenomenon not understood at present and not consistent with the sample grown at 12.5 bar. However, the overall tendency shows a systematic improvement of FWHM values with increasing reactor pressure and with this a better long range crystalline ordering in the InN epilayers. Tuna *et. al*,[4] reported a similar behavior for InN epilayers grown on GaN/Sapphire templates by low-pressure MOCVD, in the pressure range of 200 mbar to 800 mbar. The InN sample grown at 18.5 bar with a group V/III precursor ratio of 2500 shows a good long range crystalline ordering with a XRD (2θ-ω scan) FWHM value of 162.5 arcsec. Since the InN epilayers were grown on GaN/Sapphire templates of different origins, we observe a large statistical variation in the crystalline quality of the InN epilayers, as depicted in FIG. 2. Nevertheless, the overall FWHM values for the off-axis Bragg reflexes decrease with the increase of reactor pressure, a similar trend as shown in on axis crystalline order (FIG.1). The InN epilayer grown at 5 bar shows the best crystalline quality, which is attributed to the high crystalline template quality with controlled Ga-polar surface,[14] indicating a further potential to improve the quality through the use of better templates and through an improved nucleation procedure. The Raman results indicate a local optimum of the short-range crystalline ordering around 10 bar with an E_2(high) FWHM value of 10.3 cm^{-1}.

For higher reactor pressures, a slight degradation in the near-range crystalline ordering is observed, a phenomenon that might be related to higher point defect densities. To understand the discrepancies between near- and long-range crystalline ordering, further experiments in an extended process parameter field are needed.

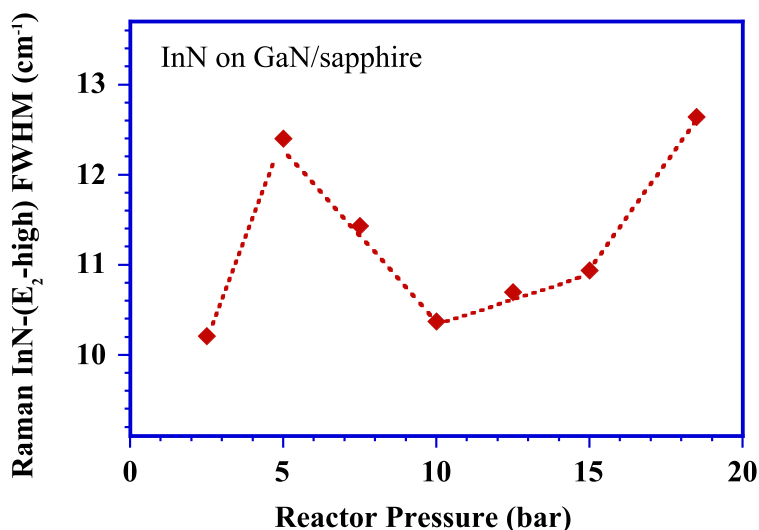

Figure 3. The FWHM of the Raman E_2(high) of the InN epilayers grown on GaN templates vs. reactor pressure.

In order to correlate and understand the relationships between the structural epilayer quality and the electrical properties as function of reactor pressure, we utilized infrared reflectance spectroscopy to analyze the InN samples. A typical FTIR reflectance spectrum for an InN-epilayer grown on a GaN/Sapphire template is shown in FIG. 4. The solid line depicts the experimental reflectance spectrum and the dotted line (color online) depicts the simulated IR reflectance spectrum for a multilayer stack, consisting of a Sapphire/GaN/InN layered structure

as depicted in the inset of FIG. 4. The multilayer stack model[15, 16] used allows the determination of the high-frequency dielectric function (ε_∞), layer thickness, as well as the free carrier concentration and mobility of the free carriers for each layer in the stack by simulating the properties for each layer and fitting it to the experimental IR-reflectance spectrum. The dielectric function of the InN layers can be modeled in the infra-red region by the lattice vibrations contribution, the free carrier contribution, and the high frequency dielectric constant ε_∞. The simulation program estimate these contributions using the Lorentz model and the classical Drude model,[17, 18] which allows to express the dielectric function for InN or GaN epilayers as

$$\varepsilon(\omega) = \varepsilon_\infty \cdot \left(1 + \frac{\omega_{LO}^2 - \omega_{TO}^2}{\omega_{TO}^2 - \omega^2 - i\cdot\omega\cdot\gamma_p} \quad \frac{\omega_p^2}{\omega^2 + i\cdot\omega\cdot\tau} \right), \tag{1}$$

where, ε_∞ is the high frequency dielectric constant, ω_{TO}, ω_{LO}, and γ_p are the TO, LO phonon frequencies and broadening parameter of the phonons, respectively. ω_p and τ are the plasma frequency and the damping constant of plasma respectively. The theoretical IR reflection spectrum is calculated using Eq. (1) and the standard multilayer stack model.[8, 9] A nonlinear fitting algorithm, utilizing a Levenberg-Marquardt approach,[19] was used to obtain the best fit parameters for each layer. To improve the reliability of the parameter set for each layer, FTIR reflection spectra were taken for the Sapphire and GaN/Sapphire templates to first establish the GaN and the sapphire parameter sets. For the simulation of the grown InN epilayers, the established GaN/Sapphire template parameters were kept constant.

The simulation results show that a single InN layer on top of the GaN/Sapphire-template structure did not converge sufficiently well, thus a second InN layer was added to improve the simulation model. This additional InN layer is assumed to capture the different properties of InN in the interfacial region at the GaN/InN interface and is related to the nucleation conditions. The inset of FIG. 4 shows the multilayer stack for the samples considered in the analysis. The plasma frequency and damping constant was extracted from the simulation for each layer, the free carrier concentration and the mobility of the free carriers were calculated using Eq. (2) and Eq. (3).

$$n_c = \frac{{\omega_p}^2 m_{eff} \varepsilon_\infty \varepsilon_0}{q^2}, \tag{2}$$

$$\mu = \frac{q}{m_{eff}\tau}, \tag{3}$$

where, n_c is the free carrier concentration, q is the electron charge, m_{eff} is the effective mass of the carriers, and μ is the free carrier mobility. The established best fit data for InN layer thickness, dielectric function, and electrical parameter for all samples grown between 2.5 and 18.5 bar reactor pressure are summarized in Table 1. The table contains two rows for each sample with the established fit parameter for the 1st - bulk (top row) and the 2nd - nucleation (bottom row) simulated two-layered stack as schematically illustrated in the inset of FIG. 4.

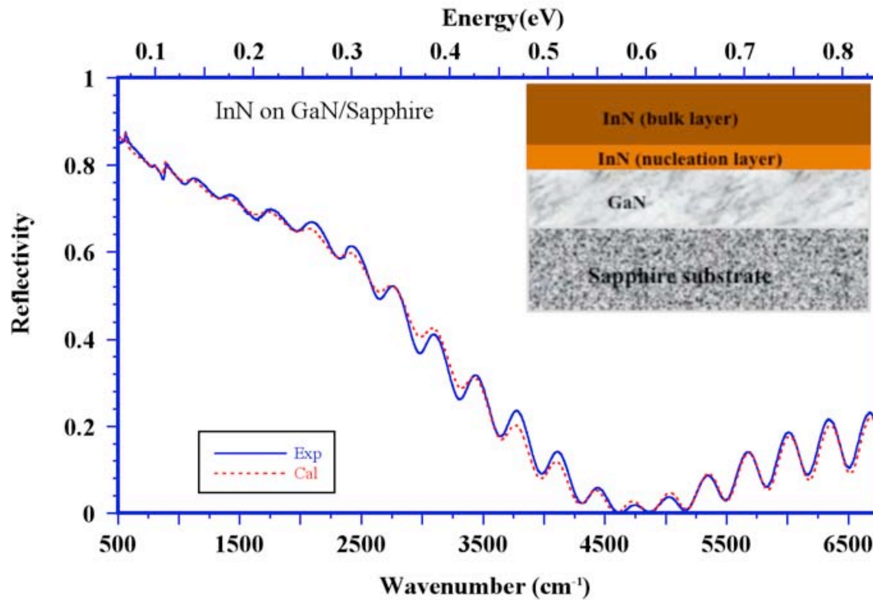

Figure 4. (color online) Experimental (solid line) and best fit (dotted line) IR reflectance spectra for an InN /GaN/ Sapphire film grown at 800 °C and 10 bar reactor pressure. Inset illustrates the layer structures were used for best fit.

Table I. InN layer parameters obtained from the best fits of FTIR reflectance spectra for InN epilayers grown are various reactor pressures. The free carrier concentration and mobilty were derived from the plasma frequency and the its damping constant, respectively. The effective mass for InN and GaN were taken constant as 0.09 m_0 and 0.2 m_0, respectively. The two rows for each sample contain the parameter for the modeled two-layered InN stack, representing the bulk (top raw) and the nucleation (bottom raw) layer of the deposited InN.

Sample	*Pressure (bar)*	*d (nm)*	ε_∞ *(high freq.)*	*Plasma freq.*(cm^{-1})	*Damping const.*(cm^{-1})	*Mobility* $(cm^2V^{-1}s^{-1})$	*Free carrier conc.* (cm^{-3})
a	*2.5*	*452.1*	*5.61*	*3720.4*	*1180.2*	*87.9*	7.78×10^{19}
		195.5	*6.03*	*4808.5*	*224.1*	*460*	1.39×10^{20}
b	*5*	*72.9*	*5.95*	*1801.3*	*1093.3*	*95*	1.94×10^{19}
		193.8	*7.44*	*4452.9*	*1210.4*	*85.7*	1.44×10^{20}
c	*7.5*	*34.1*	*5.84*	*1048*	*1033.7*	*110*	6.44×10^{18}
		325.7	*6.59*	*3710.6*	*1046.8*	*99.1*	9.11×10^{19}
d	*10*	*33.1*	*6.63*	*1316.9*	*881.1*	*120*	1.15×10^{19}
		275.8	*6.57*	*3970*	*742.2*	*140*	1.04×10^{20}
e	*12.5*	*62.2*	*6.08*	*492.4*	*378.5*	*270*	1.49×10^{19}
		189.3	*6.54*	*4286.8*	*686.2*	*150*	1.21×10^{20}
f	*15*	*10*	*7.69*	*983.9*	*872.7*	*120*	7.47×10^{18}
		307.4	*5.29*	*3543.8*	*592.5*	*180*	6.62×10^{19}
g	*18.5*	*21.2*	*7.19*	*1608.3*	*1518*	*68.4*	1.87×10^{19}
		248.5	*6.15*	*3522.2*	*485.1*	*210*	7.66×10^{19}

FIG. 5 and FIG. 6 show the computed free carrier concentrations for the InN bulk and nucleation layer as a function of reactor pressure, respectively. The free carrier concentration of the bulk layers vary from 1.5×10^{18} cm^{-3} to 7.8×10^{19} cm^{-3} and in the nucleation layers the free carrier concentration range from 6.6×10^{19} cm^{-3} to 1.5×10^{20} cm^{-3}. The lowest free carrier concentration of 1.5×10^{18} cm^{-3} was obtained for the InN bulk layer grown at 12.5 bar. These values for the bulk free carrier concentration is still higher compared to recent reported bulk free carrier concentrations of 5.6×10^{17} cm^{-3} in InN epilayers grown on GaN by plasma assisted molecular beam epitaxy (PA-MBE).[20] FIG. 6 depicts the variation of free carrier concentration in the nucleation layer as a function of the reactor pressure, indicating a slight reduction of free carrier concentration with the increasing reactor pressure. This result suggests that the reactor pressure does not significantly alter the nucleation process - and with it the free carrier concentration in the nucleation layer. Other process parameter such as the integration of a strain relaxation layer and/or optimized nuclei coalesce process have to be investigated to improve the properties of the nucleation layer. A further possible source for the high free carrier concentration may be the presence of impurities such as hydrogen and carbon,[21] which may be incorporated through an insufficient decomposition of the precursor sources. Yamamoto *et al.*[22] showed that the free carrier concentration of the bulk InN layer grown on sapphire by MBE decreases with increasing the growth temperature at two different reactor pressures, 0.1 bar and 1 bar.

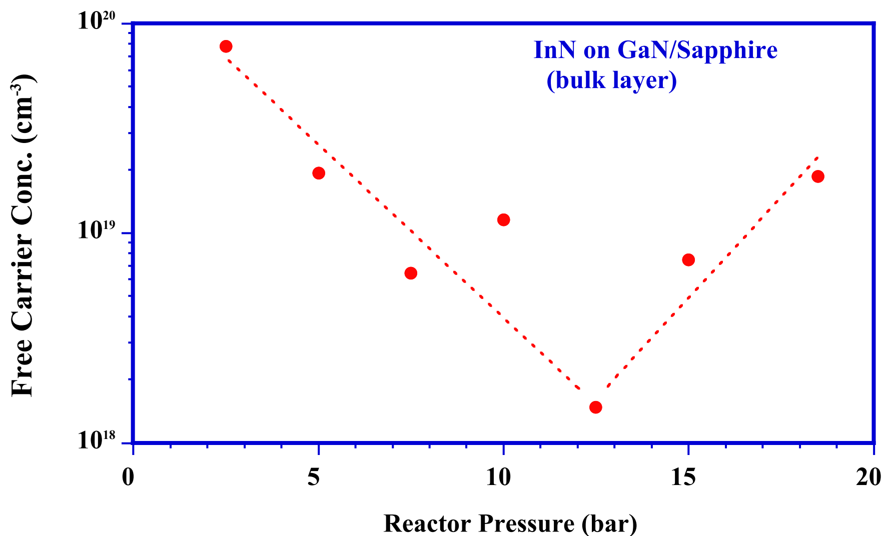

Figure 5. Dependence of free carrier concentration of InN- bulk layer on the reactor pressure.

Yamamoto *et al.*[22] also showed that InN layers grown at atmospheric pressure had a lower free carrier concentration compared to InN layers grown at lower, sub-atmospheric pressures. This indicates that increasing the reactor pressure can decrease the free carrier concentration. The results from the investigated set of InN samples indicate that for reactor pressures above 12.5 bar, the free carrier concentration increases with increasing reactor pressure, even though the crystalline quality of the epilayers improves with reactor pressure as depicted in FIG. 1. However, the trend in the free carrier concentration behavior correlates with the Raman E_{2}(high) FWHM values, indicating a possible link of point defect density with bulk free carrier concentration. Since the higher reactor pressure enables higher growth temperatures, the effective V/III precursor ratio changes due to the higher cracking efficiency of the ammonia

precursor. In this series, the group V/III precursor ratio was kept constant and has not been adjusted for the change in growth temperature with reactor pressure, which may explain the increase in the bulk free carrier concentration in the samples grown at pressures above 12 bar.

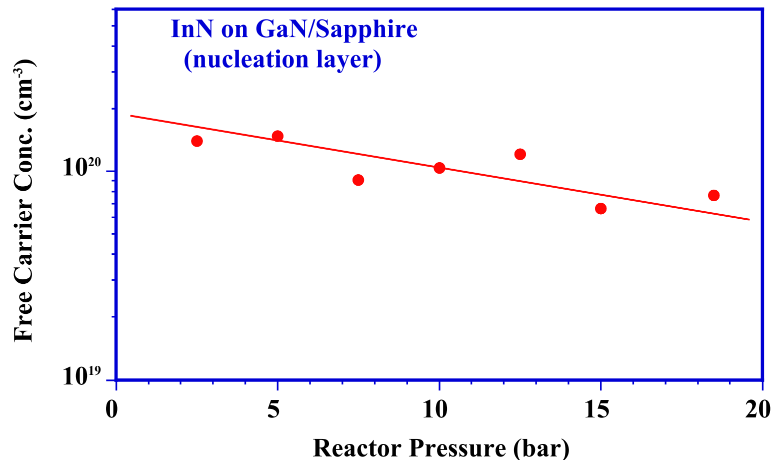

Figure 6. Dependence of free carrier concentration of InN- nucleation layer on the reactor pressure.

The mobility values for the InN bulk layer as a function of reactor pressure is depicted in the FIG. 7. These values were calculated using the Eq. (3) with the effective mass taken constant as 0.09 m_0. The mobility shows a maximum for the InN bulk layer grown with a reactor pressure of 12.5 bar, and the highest mobility of the bulk layer is found to be 270 $cm^2V^{-1}s^{-1}$. It was also observed and inverse correlation between the mobility and the free carrier concentration, as the bulk free carrier concentration shows a minimum at this pressure.

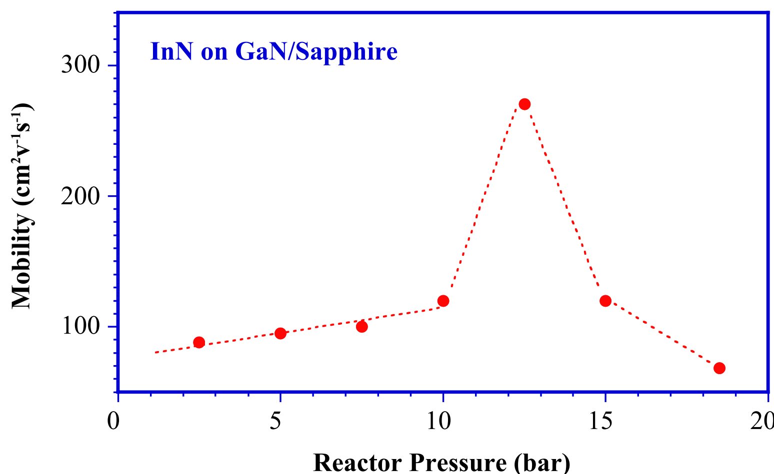

Figure 7. Mobility of the carriers of the InN bulk layer as function of reactor pressure.

The similar correlation between the mobility and the free carrier concentration has been reported by Yamamoto *et al.*[22] . In addition, Lin *et al.*[23] reported that the InN sample grown on GaN/Sapphire template by MOCVD at 675 °C has the highest mobility (1300 $cm^2V^{-1}s^{-1}$) and lowest free carrier concentration (4.6×10^{18} cm^{-3}) with the increase of growth temperature. These findings could indicate structural defects and non-intentional co-doping as sources for the high free carrier concentration, since they generate more carriers which act as scattering centers in the crystal reducing the carrier mobility. Therefore, we conclude that the free carrier mobility and

M.K.I. Senevirathna, et al. published at J. Vac. Sci. Technol. A 30, 031511 (2012) http://dx.doi.org/10.1116/1.4705727

free carrier concentration of the bulk InN layer can be further improved by adjusting the V/III precursor ratio and improving the nucleation of the InN by introducing an AlN buffer. This assumption is supported by Khan *et al*.[24] who reported a decrease in free carrier concentration and increased mobility for InN layer grown on AlN/Sapphire template with increasing V/III precursor ratio.

The InN layer thicknesses obtained from the reflectance spectra analysis were used to compute the growth rate as function of the reactor pressure. As depicted in FIG. 8, the growth rate decreases linearly with increasing reactor pressure as observed in the previous study.[12] Since the diffusion layer thickness decreases inversely proportional to the square root of the pressure, a similar behavior would be expected for the growth rate in the transport limited growth regime. The InN layer grown at 2.5 bar has a large processing error, since in our present reactor the flow channel height is fixed at 1 mm and cannot be adjusted for the variation in the diffusion layer thickness as function of the reactor pressure.

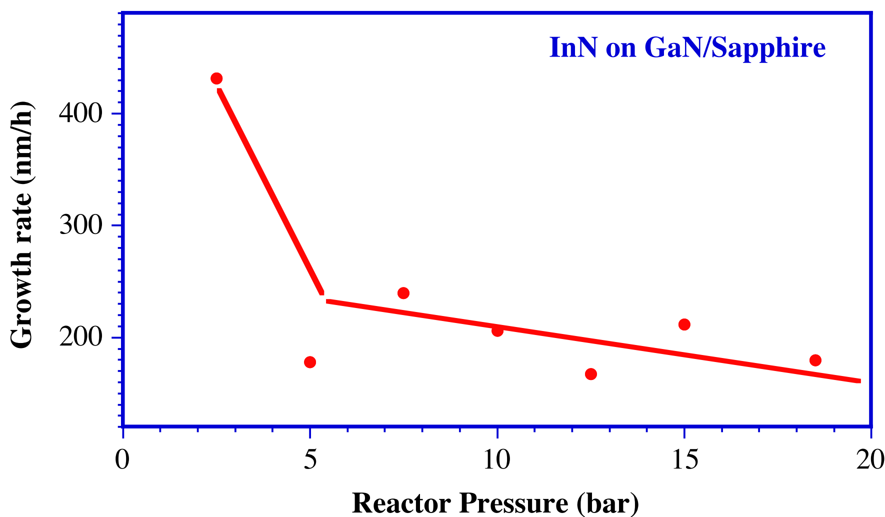

Figure 8. Growth rate as a function of reactor pressure.

IV. CONCLUSION

The reactor pressure dependent structural and electronic properties of InN epilayers have been studied. The XRD results show that the structural quality of the InN epilayers improves with increasing reactor pressure. This tendency was confirmed by the Raman results, which showed that the near-field crystallinity improves as reactor pressure increase up to 12.5 bar. Above 12.5 bar the near-filed ordering decreases, which is likely due to the higher ammonia cracking efficiency requiring adjustment of the group V/III ratio. The lowest free carrier concentration and highest mobility were found for InN grown at 12.5 bar, with values of 1.5×10^{18} cm^{-3} and 270 $cm^2V^{-1}s^1$, respectively. Further investigation are in progress in order to study the influence of the group V/III precursor ratio at higher reactor pressure and to investigate the influence of nitrogen and indium precursor fragments at the growth surface on the electrical and structural properties of the InN epilayers.

Acknowledgement

This work is financially supported by AFOSR award # FA9550-10-1-0097 and GSU-PRE

REFERENCES

[1] A. G. Bhuiyan, A. Hashimoto, and A. Yamamoto, J. Appl. Phys. **94**, 2779 (2003).

[2] D. Alexandrov, K. Scott A. Butcher, and T. L. Tansley, J. Cryst. Growth **288**, 261 (2006).

[3] D. D. Koleske, A. E. Wickenden, R. L. Henry, J. C. Culbertson, and M. E. Twigg, J. Cryst. Growth **223**, 466 (2001).

[4] Ö. Tuna, *et al.*, Phys. Status Solidi C **8**, 2044 (2011).

[5] J. B. McChesney, P. M. Bridenbaugh, and P. B. O'Conner, Mater. Res. Bull. **5**, 783 (1970).

[6] G. B. Stringfellow, J. Cryst. Growth **312**, 735 (2010).

[7] H. Lu, *et al.*, Appl. Phys. Lett. **77**, 2548 (2000).

[8] N. Dietz, in *III-Nitrides Semiconductor Materials*, edited by Z. C. Feng (Imperial College Press, 2006), pp. 203.

[9] N. Dietz, H. Born, M. Strassburg, and V. Woods, Mater. Res. Soc. Symp. Proc. **798**, Y10.45.11-14 (2004).

[10] M. Buegler, *et al.*, P. SPIE **7422**, 742218 (2009).

[11] V. Woods, H. Born, M. Strassburg, and N. Dietz, J. Vac. Sci. Technol. A **22**, 1596 (2004).

[12] Buegler, *et al.*, Phys. Status Solidi C **8**, 2059 (2011).

[13] A. R. Acharya, *et al.*, J. Vac. Sci. Technol. A **29**, 041402 (2011).

[14] N. Dietz, *et al.*, Appl. Phys. Lett. **92**, 041911 (2008).

[15] Z. G. Hu, *et al.*, Phys. Rev. B **72**, 245326 (2005).

[16] N. Dietz, Mater. Sci. Eng. **B-87**, 1 (2001).

[17] M. Alevli, A. Weerasekara, A. G. U. Perera, and N. Dietz, Appl. Phys. Lett. **89**, 112119 (2006).

[18] A. B. Weerasekara, *et al.*, J. Vac. Sci. Technol. B **26** 52 (2008).

[19] W. H. Press, S. A. Teukolsky, W. T. Vetterling, and B. P. Flannerry, in *The Art of Scientific Computing* (Cambridge U. P. , Cambrigde, MA, 1992).

[20] I. Gherasoiu, *et al.*, J. Vac. Sci. Technol. A **26**, 399 (2008).

[21] V. Darakchieva, *et al.*, Appl. Phys. Lett. **96**, 081907 (2010).

[22] A. Yamamoto, Y. Murakami, K. Koide, M. Adachi, and A. Hashimoto, Phys. Status Solidi B **228**, 5 (2001).

[23] J. C. Lin, *et al.*, Optical Materials **30**, 517 (2007).

[24] N. Khan, A. Sedhain, J. Li, J. Y. Lin, and H. X. Jiang, Appl. Phys. Lett. **92**, 172101 (2008).